

A broadband digital receiving system with large dynamic range for solar radio observation

Fa-Bao Yan^{1,2,3}, Yang Liu^{1,2}, Ke Xu², Zi-Qian Shang², Yan-Rui Su^{1,2}, Guang Lu², Yao Chen^{2,4} and Zhao Wu^{2,4}

¹ School of Mechanical, Electrical & Information Engineering, Shandong University, Weihai 264209, China

² Laboratory for Electromagnetic Detection, Institute of Space Sciences, Shandong University, Weihai 264209, China; wuzhao@sdu.edu.cn

³ CAS Key Laboratory of Solar Activities, National Astronomical Observatories, Chinese Academy of Sciences, Beijing 100101, China

⁴ Shandong Key Laboratory of Optical Astronomy and Solar-Terrestrial Environment, School of Space Science and Physics, Institute of Space Sciences, Shandong University, Weihai 264209, China

Received 2020 February 27; accepted 2020 May 7

Abstract Solar radio spectra and their temporal evolution provide important clues to understand the energy release and electron acceleration process in the corona, and are commonly used to diagnose critical parameters such as the magnetic field strength. However, previous solar radio telescopes cannot provide high-quality data with complete frequency coverage. Aiming to develop a generalized solar radio observing system, in this study, we designed a digital receiving system that could capture solar radio bursts with a broad bandwidth and a large dynamic range. A dual-channel analog-to-digital converter (ADC) printed circuit board assembly (PCBA) with a sampling rate of 14-bit, 1.25 Giga samples per second (GSPS) cooperates with the field-programmable-gate-array (FPGA) chip XC7K410T in the design. This receiver could realize the real-time acquisition and preprocessing of high-speed data of up to 5 GB s^{-1} , which ensures high time and spectral resolutions in observations. This receiver has been used in the solar radio spectrometer working in the frequency range of 35 to 40 GHz in Chashan Solar Observatory (CSO) established by Shandong University, and will be further developed and used in the solar radio interferometers. The full-power bandwidth of the PCBA in this receiving system could reach up to 1.5 GHz, and the performance parameters (DC–1.5 GHz) are obtained as follows: spur free dynamic range (SFDR) of 64.7–78.4 dB, signal-to-noise and distortion (SINAD) of 49.1–57.2 dB, and effective number of bits (ENOB) of >7.86 bit. Based on the receiver that we designed, real-time solar microwave dynamic spectra have been acquired and more solar microwave bursts with fine spectral structures are hopeful to be detected in the coming solar maximum.

Key words: instrumentation: spectrographs — techniques: spectroscopic — techniques: interferometric

1 INTRODUCTION

Solar radio emission, although excited by different emission mechanisms in different frequency ranges, always contains information of the magnetic field and plasma in the source regions in the solar corona (Gary & Keller 2004; Casini et al. 2017). In particular, the microwave bursts that are generated by gyrosynchrotron have widely been used to diagnose coronal magnetic fields (Zhou & Karlicky 1994; Kundu et al. 2004; Huang 2006; Gary et al. 2013; Nita et al. 2015; Wu et al. 2016; Kuroda et al. 2018;

Wu et al. 2019). The microwave spectrum during solar bursts usually presents as a continuum. A positive slope appears at low frequencies and a negative slope appears at high frequencies. The turnover frequency usually appears around 10 GHz (Ramaty 1969; Dulk 1985). The emission flux intensity ranges from several to thousands, or even tens of thousands of solar flux unit (SFU). However, so far, only several solar radio telescopes can provide observations covering microwave frequency ranges. For example, the Solar Broadband Radio Spectrometers (SBRS: Fu et al. 2004) which plays an

important role in solar physics research during the last solar cycle works from 0.7 to 7.6 GHz and Mingantu Ultrawide Spectral Radioheliograph (MUSER: Yan et al. 2009; Wang et al. 2013) imaging the Sun for more than 500 frequencies operates from 0.4 to 15 GHz. The Expanded Owens Valley Solar Array (EOVSA: Gary et al. 2018) covers the frequency range of 1 to 18 GHz. The Karl G. Jansky Very Large Array (VLA: Perley et al. 2011) is not solar-dedicated, although it provides complete frequency coverage from 1 to 50 GHz. Therefore, the construction of solar radio telescopes with full spectral coverage and high dynamic range is desirable.

A digital receiver is the essential instrument in a solar radio observing system, and high-speed data acquisition and real-time digital signal processing are key technologies in its design. Recently, benefiting from new signal processing devices and the trend that digitization moves toward the analog front-end and utilizes reusable, on-line configurable processors, sampling could be operated in a large bandwidth with high resolutions at the same time. These developments offer good opportunities for the construction of new facilities for solar radio observations.

In the past decade, lots of researchers have worked on this problem. The prototype of Siberian Radioheliograph (SRH: Lesovoi et al. 2012) utilized 12 bit ADC chips with the sampling rate of 100 MHz. The ADC sampling rate and resolution of Chinese heliograph - MUSER were 1 GHz and 10 bit (Liu et al. 2019), respectively. Furthermore, the Expanded Very Large Array (EVLA: McKinnon et al. 2010) could sample input signals with a 4 GHz sampler at 3 bit resolution and high dynamic signals with a 2 GHz sampler at 8 bit resolution. However, the EVLA was not solar-dedicated. In the astronomy community the Collaboration for Astronomy Signal Processing and Electronics Research (CASPER) developed Reconfigurable Open Architecture Computing Hardware (ROACH and ROACH2: Parsons et al. 2006, 2008) systems that powered over 45 scientific instruments all over the world. For instance, ADC2×1000-8 (dual 8-bit, 1000 Msps) has been used in the development of the Allen Telescope Array (ATA: Siemion et al. 2012), and ADC1×5000-8 (8-bit, 5000 Msps) has been used to design the Versatile GBT Astronomical Spectrometer (VEGAS: Chennamangalam et al. 2014) recently (refer to Hickish et al. 2016 for more details). We note that it is challengeable but important to balance the sampling rate which enables a wide bandwidth data acquisition and the resolution which determines the average system performance parameters, such as the spurious-free dynamic range (SFDR), signal-to-noise and distortion (SINAD), effective number of bits (ENOB), etc. For example, the SFDR of a 4 bit, 10 GSPS ADC designed for Greenland

Telescope (GLT) was 32.27 dB (Jiang et al. 2016), while it could reach up to ~ 59 dB for a 12 bit, 1 GSPS ADC in Chashan Solar Observatory (CSO: Du et al. 2017; Yan et al. 2017; Du et al. 2019).

To deal with the high-speed digital data from the ADC, a high-speed field-programmable-gate-array (FPGA) is needed (Ibrahim et al. 2017; Hu et al. 2019). Based on parallel computing and sufficient computing resources, the FPGA is capable of processing the complex digital data from ADCs with less time, which indicates that it is possible to realize real-time solar radio observations with high time and spectral resolutions. We note that truncating operation should be carried out on the signal of Fast-Fourier-Transform (FFT) to utilize the computing resource reasonably and retain good expendability.

Given these considerations, we have developed a digital receiver for solar radio observation, in which a printed circuit board assembly (PCBA) was designed using a dual-channel, 14-bit, 1.25 GSPS ADC AD9691 ((Analog Devices, Inc., ADI) and cooperated with the FPGA chip XC7K410T. This receiving system could capture solar radio emission in a relative wider bandwidth with better sensitivity, and has been used in a prototype of solar radio spectrometer (LEADrec2017, Laboratory for Electromagnetic Detection) which was tested for solar microwave observation in the frequency range of 35 to 40 GHz in CSO. In this observation system, solar microwave emission is captured by two circular polarized antennas (50 cm in diameter), downconverted to an Intermediate Frequency (IF) range of 937.5 ± 250 MHz by an analog circuit and sent to the receiving system. In this receiver, IF signals of both channels (left and right circular polarization) are sampled by the ADC with the bandwidth of 500 MHz and then sent to the FPGA. The LEADrec2017 will be further developed and used to observe microwave emission in relative lower frequency ranges, say, 1–5 GHz. We note that it would be a trend in the future not only in the solar community that a universal, miniaturized, modularized and standardized digital receiver could be used for observations in the entire frequency bands. Based on the LEADrec2017, we will develop an FX correlator so as to obtain high-quality real-time solar microwave dynamic spectra. So far, we have realized the preprocessing algorithms in it, such as the Finite Impulse Response (FIR), FFT, Time Delay, Cross-Correlation in Frequency Domain, etc. According to recent observing tests, the receiving system could observe microwave emission with high time and spectral resolutions, indicating that it could balance the bandwidth and sensitivity of the input signals to a large extent and could be used as a commonly used functional block in the astronomical research. The next section presents the design for the receiving system. Section 3

shows the test results. A summary is given in the last section.

2 HARDWARE DESIGN

A digital receiver for microwave observation consists of an analog to digital converter and a processor. The ADC which converts input analog signal to a digital one determines the performance of the receiving system. A large sampling rate permits the acquisition of relative wide bandwidth signal, and a high resolution can improve the sensitivity and dynamic range of a digital receiver. Therefore, a new solar radio telescope, either the spectrometer or the interferometer, which is desired to have the ability to capture solar emission in a large frequency bandwidth with increased continuum sensitivity, can be realized by adopting multi-bit, fast ADCs. We note that this selection can reduce the design complexity, cost and labor. As the final module, the processor, usually an FPGA, conducts an FFT to generate the microwave dynamic spectrum which is packaged and transmitted to the local computer by a digital signal processor (DSP). The hardware designs of this system are as follows.

2.1 Analog to Digital Converter

It has been long that the sampling rates of ADCs with high resolution range from tens to hundreds of MHz. For example, the 14 bit, 400 MHz ADC ADS5474 (Texas Instruments, TI) developed with an SFDR of ~ 67 dB was once the most cost-effective among ADCs with sample bandwidth of hundreds of MHz. Since 2010, lots of fast ADC chips have been announced, such as EV10AQ190TPY (5 GHz, 10 bit) released by Teledyne e2v, VEGA ADC30 (30 GHz, 6 bit) released by Micram, etc. Ever since then, high resolutions (12, 14 and 16 bit) have been developed for these fast ADCs. For instance, the 14 (AFE7444, TI) or even 16 (AD9081, Analog Devices) bit, 4-channel ADC chip with sampling rate of 3 GHz is now available, however, too costly. Table 1 illustrates several usually used ADCs, and we can see that the better resolution usually indicates better performance. Regarding the demands of broadband observations with large dynamic range and resolution from solar radio community, we adopt the ADC chip AD9691 (dual-channel, 1.25 GHz, 14 bit) as the essential module of the receiver system for solar microwave observation. This choice could also cut the development cost to a large extent. This device has two 14 bit cores sampling analog signals of up to 1.5 GHz. A variety of input ranges can be selected by users.

AD9691 is used to design the PCBA (see Fig. 1). The IF signal transmitted to this board from the analog-front-

end (AFE) is first transformed to a pair of differential signals by an analog circuit (see Fig. 2). Taking channel A for example, analog or clock input is transformed (1:1) to two signals (V_{in+A} and V_{in-A}) with phase difference of 180° . The cutoff frequencies for these signals are 3 GHz. The differential signals are transmitted to one of the ADC cores and process multistage, differential calculations, during which fast detections of the output and feedback will be made to monitor those input signals. The outputted signals are sent to the digital down converters (DDCs) and then the JESD204B-based high-speed serialized port (see Fig. 3).

The High-Pin-Connector (HPC) of this ADC board offers DC power connections of +1.25 V, +2.50 V, +3.30 V and +1.8 V. The pins of this connector corresponding to the digital outputs and clock signals are designed as differential pairs with impedances of 50Ω for a single-end and 100Ω for differential ones. This connector provides totally 20 gigabit interfaces (data pairs, DP) which could transmit 10 differential inputs and outputs simultaneously. The data transmitting speed can reach up to 10 Gbit. The AD9691 is configured to use two converters and four lanes by default. Therefore, Converter A data are outputted to SERDOUT0 \pm to SERDOUT3 \pm , and Converter B data are outputted to SERDOUT4 \pm to SERDOUT7 \pm (see Fig. 3). The parallel data processed by the ADC chip is assembled and encoded with an 8/10B encoding by the JESD204B data transmit block to form serial output data which will be further processed by the FPGA. The PCBA (see Fig. 1) follows the ANSI/VITA (FMC) standard and it could be convenient to plug compatibly with the FPGA board.

2.2 Processor

The digitalized microwave emission signal is finally transmitted to the FPGA to generate the dynamic spectrum, during which a Hanning window, an FFT as well as integrations over time and frequency domains are conducted (see Fig. 4). The results are further processed by the DSP and outputted to the host computer.

We note that the Hanning window is used to reduce the spectrum leakage. We perform an FFT for every 8 k samples, and therefore the spectral resolution can reach 156 kHz, which indicates fine structures can be observed in the dynamic spectrum. The modulus operation is then carried out over in-phase (I) and quadrature (Q) signals to yield the magnitude of the spectrum. Integrations can be operated both in time and frequency domains, which reduce the amount of data greatly and at the same time make the magnitude of spectrum more stable. The dynamic spectrum is finally packaged with timestamp and transmitted through GigE network to the users.

Table 1 Comparison of Performance-Price of Commonly Used ADCs

No.	Chip	Sampling Rate (GSPS)	Resolution (bit)	f_{in} (MHz)	SFDR	SNR	Price (USD)
1	ADS5474	0.4	14	230	80 dBc	69.8 dBFS	>195
2	AD9694	4-CH 0.5	14	985	79 dBFS	66 dBFS	>575
3	ADS54J40	2-CH 1.0	14	350	75 dBc	66.3 dBFS	>515
4	AD9680	2-CH 1.0	14	985	80 dBFS	61.4 dBFS	>688
5	ADS54J60	2-CH 1.0	16	350	75 dBc	67.5 dBFS	>620
6	AD9691	2-CH 1.25	14	985	72 dBFS	59.7 dBFS	>815
7	ADC10D1500	2-CH 1.5 1-CH 3.0	10	748	65 dBc 59 dBc	55 dBFS 52.1 dBFS	>1915
8	EV10AQ190AVTPY	4-CH 1.25 2-CH 2.5 1-CH 5.0	10	1200	65dBc 56dBc 56 dBc	48dBFS 47.5 dBFS 47.5dBFS	~1400



Fig. 1 The dual-channel 14 bit, 1.25 GSPS ADC board. The SMA connectors (from top to bottom) on the right side of the board are for signal input (ch-A, DC to 1.5 GHz), external clock (100 MHz or 1.5 GHz), external triggering input and signal input (ch-B, DC to 1.5 GHz), respectively. The triggering signal can be either 1 pps signal from external triggering input connector or clock signal from the HPC connector. The digital signals processed by the ADC chip AD9691 (beside the LED) are outputted from the connector of JESD204B on the left side of the board.

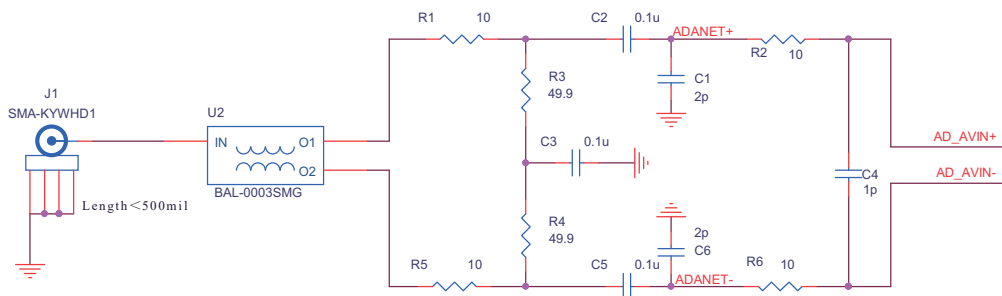


Fig. 2 Analog input circuit for AD9691.

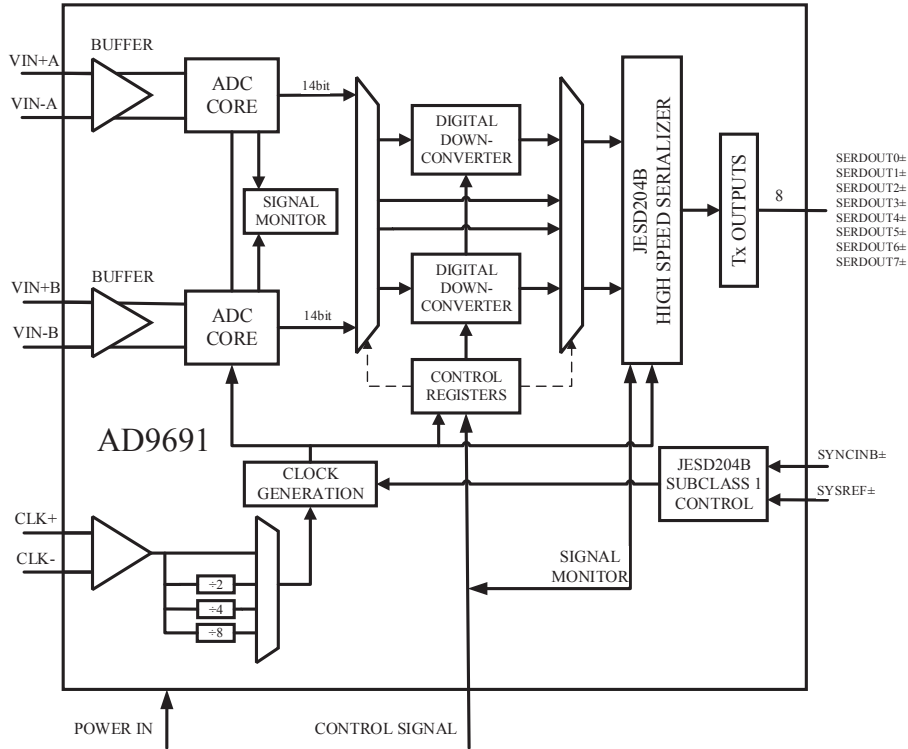


Fig. 3 Function block diagram of AD9691 (ADI 2015).

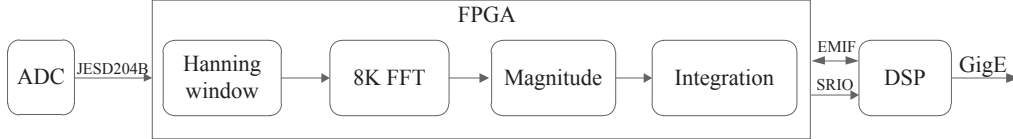


Fig. 4 Digital signal process in the receiving system.

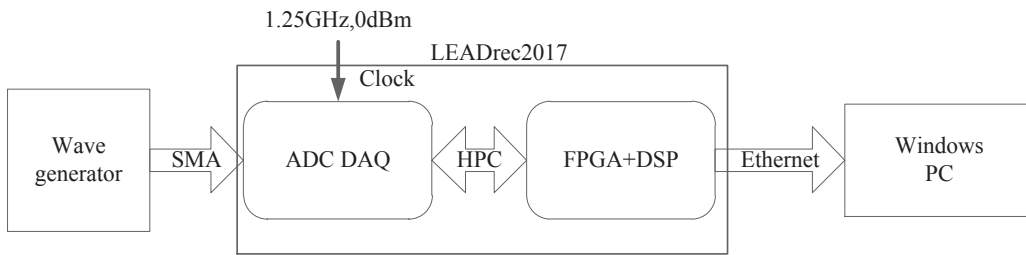


Fig. 5 Test setup for the receiving system.

3 PERFORMANCE AND APPLICATION

So far, the receiving system has been tested in the laboratory (the corresponding test configuration is shown in Fig. 5) and used for observations of solar microwave emission.

3.1 Performance

As the essential part of the receiver, the analog-to-digital module determines the main performance of the system,

and tests are therefore first carried out for it using signals of specific frequencies and broadband signals generated by signal generator N5183B (Keysight) and vector signal generator SMW200A (Rohde & Schwarz), respectively. These signals are processed by the receiving system and dynamic spectra are then outputted to the local PC. We have performed tests in a frequency range of 20 MHz to 2.5 GHz, and the performance are obtained and shown in Figure 6. To reduce frequency aliasing, the receiving system is designed to work in the frequency range of 687.5 MHz to

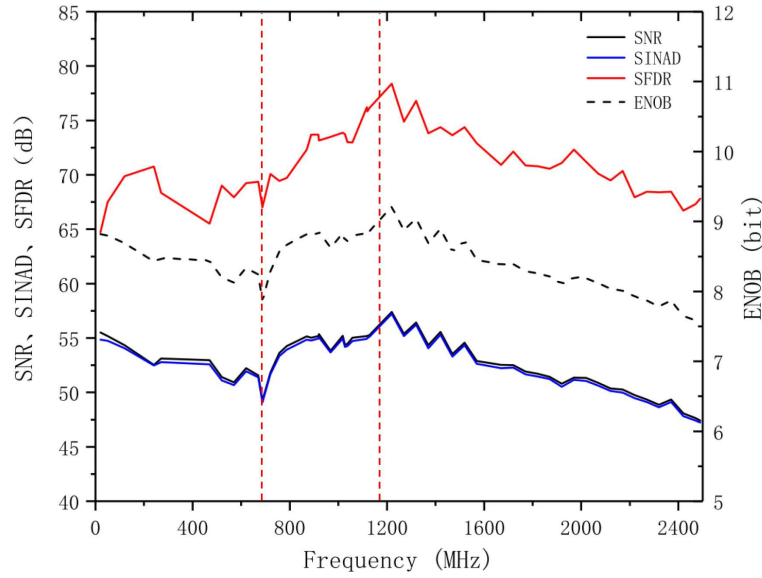


Fig. 6 Performances of receiving system at a -1 dBfs drive in the frequency range of 20 MHz to 2.5 GHz. The *black*, *blue* and *red* lines represent the SNR, SINAD and SFDR performances, respectively. The *dashed* line represents the ENOB performance. The *plots* in between the *vertical dashed* line denote the performance of the receiving system in the designed frequency range (687.5 MHz – 1.1875 GHz).

1.1875 GHz, and the performance in this frequency range are marked in between the vertical red dashed lines.

The SNR is defined as the ratio of input signal power to the noise power. The tested SNR for the receiving system is shown as the black solid line in Figure 6. We can see that the SNR (input signal drive at -1 dBfs) presents a decreasing-increasing trend with the increasing frequency in the frequency range of 20 MHz–1.2 GHz, and an overall decreasing trend above ~ 1.2 GHz. These values remain above the level of ~ 47 dB. For instance, SNRs at 120 MHz, 1.12 GHz and 2.02 GHz are 54.34, 55.20 and 51.32 dB, respectively. In the working frequency domain of the receiving system, the SNR plot illustrates a smooth and slight increasing tendency when the frequency changes from 687.5 MHz to 1.1875 GHz, and the SNR is around 49–55 dB.

We note that measured SNR is usually smaller than the theoretical one, and this is because the noise level is affected by the harmonic distortion, quantization noise as well as the thermal noise in the test. Therefore, we further test the SINAD of this system. The SINAD is usually written as the ratio of the maximum amplitude of the signal to the system-producing noise and distortion, and is an important asset of the systematic dynamic range. We plot the measured SINAD as the blue solid line in Figure 6. As shown in this figure, the SINAD stays in the range of 47.2 to 57.2 dB from 20 MHz to 2.5 GHz and in the range of 49.1 to 57.2 dB in the full-power-bandwidth (DC to 1.5 GHz). These values are slightly smaller than SNR. The SINAD of the receiving system in its designed frequency range (in

between the red dashed lines) remains stable and around 50 dB. Specifically, at 687.5 MHz, $\text{SINAD}_{\min} = 49.1$ dB and at 1.1375 GHz, $\text{SINAD}_{\max} = 55.6$ dB. This indicates the dynamic range in this frequency range permits a high quantity solar microwave observation.

The ENOB is closely related to the SINAD, and the relationship between them can be written as (Jiang et al. 2014):

$$\text{ENOB} = (\text{SINAD} - 1.76 \text{ dB}) / 6.02 \text{ dB}. \quad (1)$$

Therefore, similar to the frequency dependence of the SINAD, the ENOB also presents a mild change with the changing frequency (see the dashed line in Fig. 6). We note that the ENOB can illustrate the performance intuitively. In the testing frequency range, the ENOB remains larger than 7.55 bit and it is greater than 7.86 bit in the frequency range of 687.5 MHz to 1.1875 GHz with a maximum of 8.95 bit around 1.1375 GHz.

The SFDR is the ratio of the fundamental signal power to the strongest harmonic signal power, and it is usually used to quantize the system distortion. As seen from Figure 6, the SFDR (red solid line) ranges from ~ 64.7 dB to ~ 78.4 dB, indicating a large dynamic range and good working state for the ADC device and the receiving system. We note that there are relative large fluctuations of the SFDR values with the increasing frequency, and this is due to the influence of various noises in the test.

According to these tests, the performance parameters of the receiving system are good enough for its application in solar radio observations. The larger SNR over 50 d-

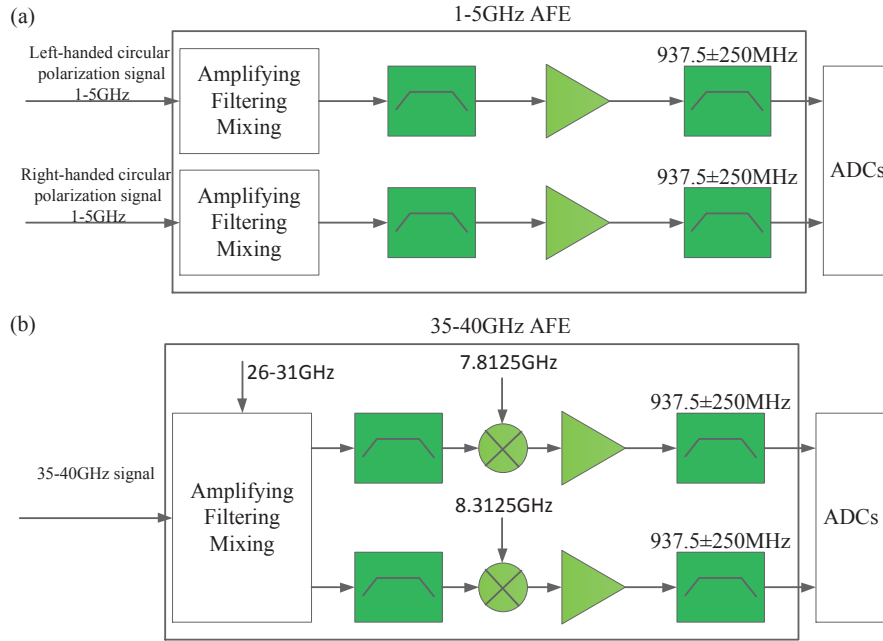


Fig. 7 The diagram for the downconverter before the digital receiver for radio spectrometers working in different input frequency ranges. The upper (*bottom*) diagram represents the design for input signals in the frequency range of 1.0 to 5.0 GHz (35.0 to 40.0 GHz). (a) The input signals (1.0–5.0 GHz) of both left and right polarization are filtered and downconverted to a IF ranging from 687.5 to 1187.5 MHz and are then transmitted to the ADC chip AD9691 simultaneously. (b) The input signals (35.0–40.0 GHz) of either polarization are divided into two 500 MHz-wide channels after the initial mixing operation (LO of 26–31 GHz), and then mixed to the IF of 937.5 ± 250 MHz. Both diagrams use time-sharing configurations.

B indicates that influence from noise can be reduced by a large extent in the conversion of the analog signal to a digital one. The larger SINAD or ENOB permits the device to capture tiny and strong signal simultaneously, and the good performance of SFDR ensures the sensitivity at the same time.

3.2 Applications

The receiving system has been used to design solar microwave spectrometers cooperating with an AFE. The microwave emission captured by antennas is first sent to the AFE which amplifies, filters and downconverts the observed signal to the working frequency range of the ADC selected. The down-converting circuits for the spectrometers in the frequency range of 1.0–5.0 GHz (upper, under design) and 35.0–40.0 GHz (bottom) systems are shown in Figure 7.

In the low frequency system (see Fig. 7(a)), both left and right polarized radio emissions are acquired by a single dual-circular-polarized antenna. The signals are then processed in separate channels. Signal with either polarization is amplified, filtered and finally mixed to the IF of 937.5 ± 250 MHz (bandwidth of 500 MHz). And therefore eight times of cycles are needed to sample the radio emission ranging from 1.0 to 5.0 GHz. As seen from

Figure 7(b), signal ranging from 35 to 40 GHz with either polarization is acquired and processed by a high-frequency system. An 1 GHz-wide sampling is conducted, and therefore, five successive cycles are needed to cover the observing frequency range. This signal is first mixed by local oscillation (LO, 26–31 GHz), and then divided into two 500 MHz-wide signals which will be processed in separate channels. These signals are finally downconverted for the second time to the IF of 937.5 ± 250 MHz and sent to the ADC cores. According to the above designs, we can reduce the cost and complexity of the entire observation system, while capturing larger portions of microwave spectrum.

We have manufactured a spectrometer working in the frequency range of 35 to 40 GHz, and the prototype is shown in Figure 8. The tests of signals at specific frequencies and entire bandwidth have been carried out by a signal generator and a vector signal generator, respectively. Figure 9 presents the dynamic spectrum observed by this spectrometer on 2020 January 15, and obviously the flux density decreases gradually during the sunset after $\sim 08:00$ UT. No events have been observed yet due to the solar minimum. We note that these values are normalized to those at 06:40 UT and the calibration for the observation system is now in progress.

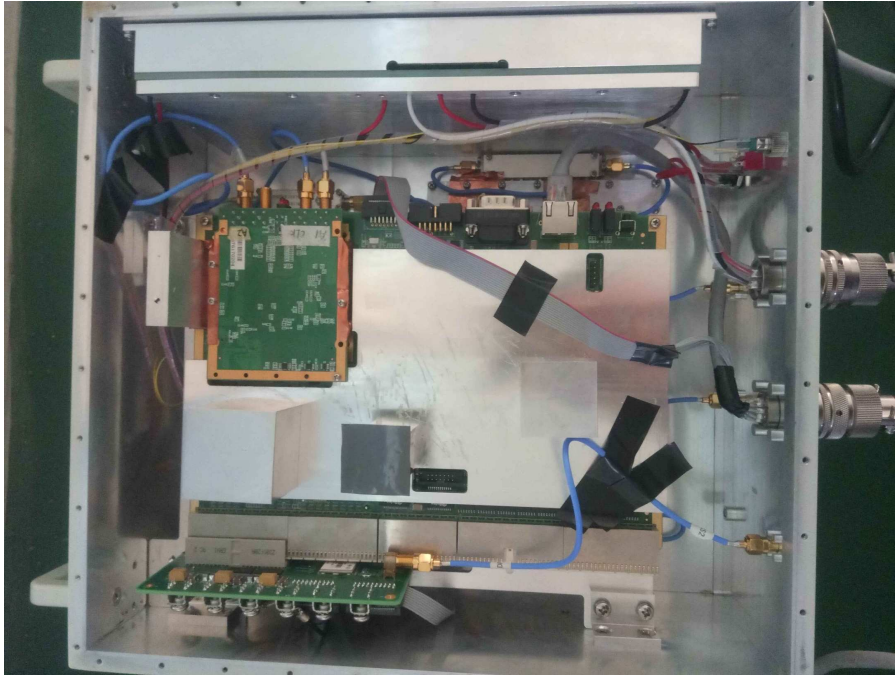


Fig. 8 The prototype of a spectrometer developed by CSO working in the frequency range of 35–40 GHz.

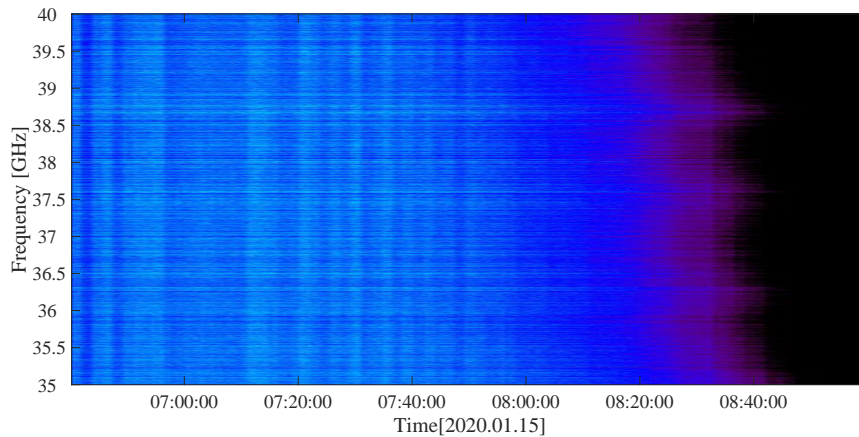


Fig. 9 The dynamic spectrum observed on 2020 January 15 by the 35–40 GHz spectrometer in Chashan Observatory. The microwave emission flux density decreased after $\sim 8:00$ UT due to the increasing absorption of the atmosphere at lower solar elevation during the sunset. At 08:42 UT, the antenna of the observing system began to point away from the Sun. The flux densities are normalized to the corresponding values at 06:40 UT.

4 SUMMARY

Solar radio emissions during solar bursts contain valuable information of the coronal magnetic field, plasmas and energetic particles in the source region. Therefore, solar radio observations are of importance for the study of the physics of solar bursts. So far, solar radio instruments, such as spectrometers, heliographs etc., mainly work in low frequency regime (metric to decametric wave). In the high frequency regime (centimetre to decimetric wave), only several solar radio arrays (e.g., EOVS, MUSER, NoRH; Nakajima et al. 1994) could supply observation data rou-

tinely. However, there are persisting demands from solar community for a full frequency coverage of the solar radio observations.

The essential issue for the construction of new radio telescopes focuses on the design and manufacture of the data processing system. For better observation, the high time resolution, high frequency resolution together with high sensitivity are desired in this newly-developed system. Therefore, the selections of a fast ADC chip with large sensitivity at a reasonable cost, together with a digital processor with sufficient computing resource are of significance.

Given these considerations, in this study, we design and manufacture a broadband digital receiving system with large dynamic range which can be used for solar microwave observation. In this system, ADC chip AD9691 is used to design a PCBA which could sample input signal of up to 1.25 GHz (FPBW up to 1.5 GHz) at a 14 bit resolution. This PCBA collaborates with a fast FPGA chip XC7K410T to realize real-time solar microwave emission acquisition and processing.

Tests have been carried out for this receiving system, and the performance parameters were obtained in the testing frequency range of 20 MHz–2.5 GHz. The SINAD ranges from 47.2 to 57.2 dB, and the ENOB is therefore in a range of 7.55–9.21 bit. The SNR is slightly larger than SINAD. The SFDR ranges from 64.7 to 78.4 dB. These performance parameters ensure that the data processing system can capture input signals with a large dynamic range for a relative larger frequency bandwidth.

This receiving system has been used to manufacture the microwave spectrometer working in the frequency range of 35 to 40 GHz (the design of AFE is shown in Fig. 7(b)), which is now in trial operation in CSO. It will be used to design the low-frequency spectrometer and interferometer (1–5 GHz). We will further develop this receiving system to be a modularized block in the construction of next-generation radio telescopes, and it is hopeful to play an important role in the observation of microwave bursts in the coming solar maximum.

Acknowledgements This work is supported by the National Natural Science Foundation of China 11703017, 11790303 (11790300), 11803017, 41774180, 41904158, 11973031, the China Postdoctoral Science Foundation (2019M652385), Open Research Program CAS Key Laboratory of Solar Activity, National Astronomical Observatories (KLSA201907) and Young Scholars Program of Shandong University, Weihai (20820201005).

References

- Analog Devices, 2015, 14-Bit, 1.25 GSPS JESD204B, Dual Analog-to-Digital Converter, AD9691, <https://www.analog.com/media/en/technical-documentation/data-sheets/AD9691.pdf>
- Casini, R., White, S. M. & Judge, P. G. 2017, *Space Sci. Rev.*, 210, 145
- Chennamangalam, J., Scott, S., Jones, G., et al. 2014, *PASA*, 31, e048
- Du, Q., Cheng, R., Chen, C., et al. 2019, *Scientia Sinica (Technologica)*, 49, 901 (in Chinese)
- Du, Q. F., Chen, L., Zhao, Y. C., et al. 2017, *RAA (Research in Astronomy and Astrophysics)*, 17, 111
- Dulk, G. A. 1985, *ARA&A*, 23, 169
- Fu, Q., Ji, H., Qin, Z., et al. 2004, *Sol. Phys.*, 222, 167
- Gary, D. E., Chen, B., Dennis, B. R., et al. 2018, *ApJ*, 863, 83
- Gary, D. E., Fleishman, G. D., & Nita, G. M. 2013, *Sol. Phys.*, 288, 549
- Gary, D. & Keller, C. 2004, *Astrophysics and Space Science Library*, 314, eds. Dale E. Gary et al. (Dordrecht: Kluwer Academic Publishers)
- Hickish, J., Abdurashidova, Z., Ali, Z., et al. 2016, *J. of Astronomical Instrumentation*, 05, 1641001
- Hu, X., Wei, L., & Chen, Y. 2019, *Ordance Industry Automation*, 38, 39 (in Chinese)
- Huang, G. 2006, *Sol. Phys.*, 237, 173
- Ibrahim, A., Gastaldo, P., Chile, H., et al. 2017, *Sensors (Basel)*, 17, 558
- Jiang, H., Liu, H., Guzzino, K., et al. 2014, *PASP*, 126, 761
- Jiang, H., Yu, C., Kubo, D., et al. 2016, *PASP*, 128, 115002
- Kundu, M. R., Nindos, A. & Grechnev, V. V. 2004, *A&A*, 420, 351
- Kuroda, N., Gary, D. E., Wang, H., et al. 2018, *ApJ*, 852, 32
- Lesovoi, S. V., Altyntsev, A. T., Ivanov, E. F., et al. 2012, *Sol. Phys.*, 280, 651L
- Liu, F., Yan, Y., Wang, W., et al. 2019, *PASA*, 36, e043
- McKinnon, M., Perley, R., Jackson, J., et al. 2010, in *Ground-based and Airborne Telescopes III*, Proc. SPIE, 7733, 77331A
- Nakajima, H., Nishio, M., Enome, S., et al. 1994, *IIEEP*, 82, 705
- Nita, G. M., Fleishman, G. D., Kuznetsov, A. A., et al. 2015, *ApJ*, 799, 236
- Parsons, A., Backer, D., Siemion, A., et al. 2008, *PASP*, 120, 1207
- Parsons, A., Backer, D., Chang, C., et al. 2006, *ACSSC06*, 2031, doi: 10.1109/ACSSC.2006.355123
- Perley R. A., Chandler C. J., Butler B. J., Wrobel J. M. 2011, *ApJ*, 739, L1
- Ramaty, R. 1969, *ApJ*, 158, 753
- Siemion, A. P. V., Bower, G. C., Foster, G., et al. 2012, *ApJ*, 744, 109,
- Wang, W., Yan, Y., Liu, H., et al. 2013, *PASJ*, 65, s18
- Wu, Z., Chen, Y., Huang, G., et al. 2016, *ApJ*, 820, L29
- Wu, Z., Chen, Y., Ning, H., et al. 2019, *ApJ*, 871, 22
- Yan, F. B., Liu, J. X., Su, Y. R., et al. 2017, *Chinese J. Geophys.*, 60, 4204, doi: 10.6038/cjg20171108 (in Chinese)
- Yan, Y., Zhang, J., Wang, W., et al. 2009, *Earth Moon and Planets*, 104, 97
- Zhou, A. H., Karlický, M. 1994, *Sol. Phys.*, 153, 441